Acta Crystallographica Section A
Foundations of Crystallography
ISSN 0108-7673

Received 3 December 2007
Accepted 28 February 2008

X-ray structure refinement using aspherical atomic density functions obtained from quantum-mechanical calculations

Dylan Jayatilaka[a] and Birger Dittrich[b]*

[a]Chemistry, School of Biomedical and Chemical Sciences, The University of Western Australia, Crawley 6009, Australia, and [b]Institut für Anorganische Chemie der Universität Göttingen, Tammannstrasse 4, Göttingen, D-37077 Germany. Correspondence e-mail: bdittri@gwdg.de

An approach is outlined for X-ray structure refinement using atomic density fragments obtained by Hirshfeld partitioning of quantum-mechanical density fragments. Results are presented for crystal structure refinements of urea and benzene using these 'Hirshfeld atoms'. Using this procedure, the quantum-mechanical non-spherical electron density is taken into account in the structural model based on the conformation found in the crystal. Contrary to current consensus in structure refinement, the anisotropic displacement parameters of H atoms can be reproduced from neutron diffraction measurements simply from a least-squares fit using the Hirshfeld atoms derived from the BLYP level of theory and including a simple point-charge model to treat the crystal environment.

1. Introduction

In most cases, a crystal structure – by which we mean the atomic positions and atomic displacement parameters (ADPs) – is obtained from X-ray diffraction experiments using the promolecule model. This model approximates the electron density (ED) in the crystal as a sum of spherically symmetric atomic density functions (ADFs) obtained from quantum-mechanical (QM) calculations. However, it is well known that asphericity in the atomic density can be detected. For example, for typical small organic molecules, at least half of the measured reflections will show changes greater than 1% due to deficiencies in the promolecule approximation, and changes of up to 20% are often observed (Bytheway *et al.*, 2007). Accordingly, in X-ray charge-density refinement, one attempts to model the asphericities and obtains an improved description of the crystal structure. In charge-density refinement, the ED in the crystal is approximated as a sum of ADFs which are allowed to be aspherical, the asphericity being described by multipole expansion parameters. The aspherical ADFs modelled in this way have been called pseudoatoms (Stewart, 1976), and the treatment of high-resolution X-ray single-crystal diffraction data using the pseudoatom formalism is most often carried out using the Hansen–Coppens variant of the multipole model (Hansen & Coppens, 1978). It is a mature technique in charge-density refinement (Coppens, 2005).

In this paper, an alternative approach to X-ray crystal structure refinement is considered. Instead of modelling the experimental data using the promolecule model or the pseudoatom model, we propose to obtain aspherical ADFs from a better QM model. Specifically, we propose to obtain the aspherical ADFs by Hirshfeld's stockholder partitioning (Hirshfeld, 1977) of an electron density obtained from QM calculations. For convenience, we henceforth call such aspherical ADFs 'Hirshfeld atoms' (HAs).

The idea to use HAs is not without precedent: Bruning & Feil (1992) and Koritsánszky & Volkov (2004) have also used them. However, in the former case the method was used to calculate thermally averaged structure factors while in the latter case the authors used the further approximation of representing the HAs within the pseudoatom formalism (Koritsánszky & Volkov, 2004). By contrast, in this work, we propose to use the HAs directly without further approximation. Since our interests are with molecular crystals, we obtain the HAs from isolated-molecule QM calculations, assuming that these HAs are representative of an atomic fragment of the ED in the crystal. As far as we are aware, no-one has yet used such atoms in a crystal structure refinement against X-ray data.

There are several motivations for the work described here, which are now discussed.

One motivation is to see what the differences in the refined structure parameters are, compared with established charge-density refinement techniques and compared with results from neutron diffraction experiments. A second motivation is to see if H-atom positions and ADPs can be obtained using this new model. To obtain accurate H-atom positions from X-ray diffraction data is an almost historical problem which Stewart & Bentley (1975) suggested could be solved by introducing a finite multipole expansion of the charge density for the H atom taken from the same atom in the H_2 molecule. Such an idea has been applied by, for example, Destro & Merati

(1995). However, while obtaining H-atom positions is possible, obtaining the corresponding ADPs is much more difficult unless additional assumptions and measurements are used. For example, Madsen *et al.* (2004) have obtained the ADPs for H atoms in good agreement with those from neutron diffraction experiments by using a model which itself uses the neutron ADPs from a variety of related structures. On the other hand, one can avoid this somewhat tautological approach if some of the ADP information is obtained from QM vibrational calculations (Whitten & Spackman, 2006). By contrast with these conceptually complicated approaches, in this paper the H-atom ADP information is obtained only from the X-ray data using an improved electron-density model.

In the proposal we have outlined, a QM calculation is required after a preliminary X-ray structure refinement. This QM calculation will be time consuming at best and impractical at worst. However, if it were possible to derive transferable atomic density fragments (TADs), then the scheme we have outlined could be applied in a practical way. By 'transferable', we mean that the same aspherical ADF is used for atoms which are in the same chemical environment (after a suitable alignment procedure). Jelsch, Volkov and Dittrich, and their co-workers, have independently developed different schemes for TADs, using the pseudoatom formalism to represent the ADFs (Pichon-Pesme *et al.*, 1995; Volkov *et al.*, 2004; Dittrich *et al.*, 2004, 2006; Zarychta *et al.*, 2007; Dominiak *et al.*, 2007). In the case of Dittrich and co-workers, and Volkov and co-workers, theoretical calculations were used to obtain the TADs, which have been termed invarioms or pseudoatom database parameters, respectively.

In view of the work just described, a third motivation for the work described here is to facilitate developing quantum-mechanical TADs. Such a development would (*a*) eliminate the problems of trying to represent the electron density using only a limited number of atomic functions, as is done in the pseudoatom formalism, and (*b*) also eliminate the need for an expensive QM calculation before a structure refinement. We will pursue the development of QM invarioms in future work. In Fig. 1, we have tried to give an overview of the different structure refinement models currently in use and their relationship to each other.

Even though the Hirshfeld-atom model we propose is better than the promolecule model, such HAs will (by definition) not include the effects of intermolecular interactions. The adequacy of the isolated-molecule model depends entirely on whether the interaction density is observable in the measured structure factors. Should such intermolecular interaction effects be important, the structural parameters obtained from the approach we have outlined would serve as a good starting point for X-ray constrained Hartree–Fock (XCHF) modelling (Jayatilaka, 1998; Grimwood & Jayatilaka, 2001; Grimwood *et al.*, 2003). A previous study on oxalic acid, for example, suggested that an inability to obtain a good χ^2 agreement statistic when using the XCHF model was due to small errors in positional and ADP parameters (Grimwood & Jayatilaka, 2001).

A fourth motivation for this paper is, therefore, a desire to obtain more accurate structural parameters for the XCHF model, with the ultimate aim of obtaining an improved description of the interaction density, the effect of the surrounding molecules in the crystal on the electron density of the isolated molecule [for a definition of the interaction density see *e.g.* Spackman *et al.* (1999)]. The interaction density contributes to the electrostatic part of the intermolecular interaction energy, and hence to the binding energy of the crystal, an important physical quantity.

The outline of the paper is as follows. In the following section, we present the necessary theory for refining X-ray structures using Hirshfeld-partitioned ADFs obtained from QM calculations on isolated-molecule molecular densities. Subsequently, we apply and test our method on crystal structures of urea and benzene.

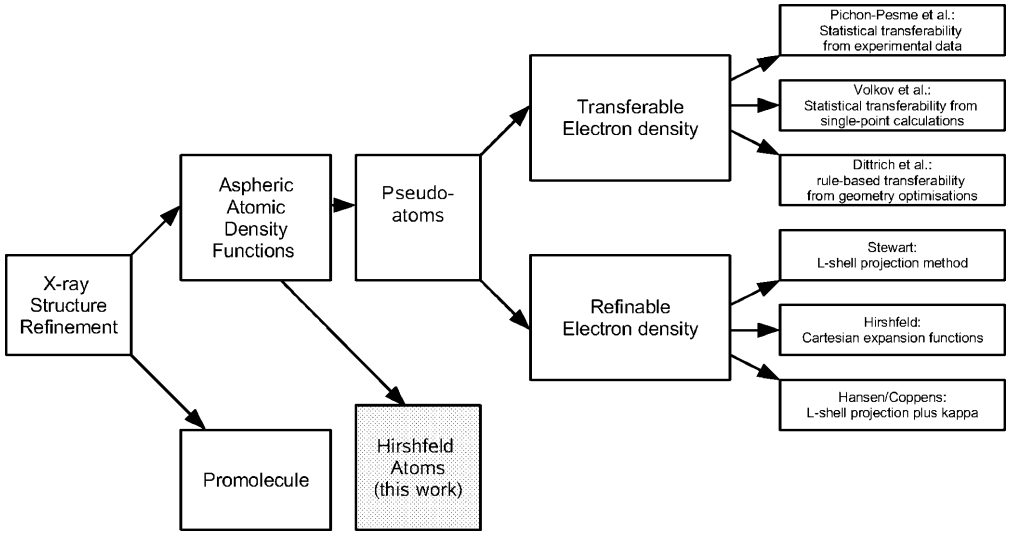

Figure 1
Overview of structure refinement models.

2. Theory and details of implementation

In this section, we present a brief exposition of structure refinement based on HAs. The key concepts and steps involved are outlined below, including some comments on details of efficient implementation and other approximations used, notably the rigid-Hirshfeld-atom approximation. The new method is introduced with a comparison to the standard multipole model.

2.1. Multipole model *versus* quantum-chemical electron-density expressions

In the multipole model, the electron density $\rho(\mathbf{r})$ is described by an analytical expression based on the sum of rigid *atom-centered* multipole functions in terms of multipole parameters κ, κ', P_v and P_{lm},

$$\rho_{\rm atom}(\mathbf{r}) = \rho_{\rm core}(r) + P_v\kappa^3\rho_v(\kappa\mathbf{r}) + \rho_{\rm deformation}(\mathbf{r}), \quad \text{with}$$
$$\rho_{\rm deformation}(\mathbf{r}) = \sum_{l=0}^{l_{\rm max}} \kappa'^3 R_l(\kappa'\mathbf{r}) \sum_{m=0}^{l} P_{lm\pm}\, d_{lm\pm}(\theta,\phi). \tag{1}$$

The multipole parameters can be refined by least-squares methods using experimental data or predicted by theory *via* simulated structure factors (Koritsanszky *et al.*, 2002). Core and spherical valence densities (ρ_v) of the heavy atoms are composed of Hartree–Fock wavefunctions expanded over Slater-type basis functions. For the deformation terms, single-ζ orbitals with energy-optimized Slater exponents are employed and kept fixed (Clementi & Roetti, 1974).

By contrast with the atom-centered model employed in the multipole model, in quantum mechanics a two-center electron-density description is used, and the basic unit is not the atom but a molecule. Usually the $\rho_{\rm molecule}$ is

$$\rho_{\rm molecule}(\mathbf{r}) = \sum_{A,B}\sum_{i,j} D_{ij}^{AB} f_i(\mathbf{r}) f_j(\mathbf{r}). \tag{2}$$

Here D_{ij}^{AB} is the density matrix (typically obtained in a quantum-chemical calculation) and f_i, f_j are the basis functions centered on the atoms A and B, respectively. These basis functions are typically linear combinations of several Gaussian functions and are therefore much more flexible than those used in the multipole representation. An important difference between equation (2) and equation (1) is that the latter requires two atomic centers A, B. While this allows the calculation of quantities such as the kinetic energy, which is not possible using the pseudoatom formalism, the use of equation (2) does cause difficulties when calculating thermally averaged structure factors which require an atom-centered formalism. The Hirshfeld-atom scheme proposed in this work circumvents this problem.

2.2. Hirshfeld atoms

Assume that the crystal is composed of a single molecule or molecular fragment whose electron density is $\rho_{\rm molecule}(\mathbf{r})$. Now assume that $\rho_{\rm molecule}(\mathbf{r})$ can be approximated by an isolated-molecule QM calculation, such as given in equation (2). The choice of this molecule is not unique, and different choices may be better or worse (Jayatilaka & Grimwood, 2001; Grimwood & Jayatilaka, 2001). To build up $\rho_{\rm cell}(\mathbf{r})$, the electron density in the unit cell, our strategy is to carve up the molecular density $\rho_{\rm molecule}(\mathbf{r})$ into aspherical atomic density functions which can be copied by symmetry operations to the appropriate positions in the unit cell. To do this, we will use the Hirshfeld partitioning technique.

Hirshfeld has defined the density of an atom at its position $\mathbf{r}_A$ in a molecule by (Hirshfeld, 1977)

$$\rho_A(\mathbf{r}) = w_A(\mathbf{r})\rho_{\rm molecule}(\mathbf{r}). \tag{3}$$

In what follows, we shall call this the Hirshfeld atom. The weight function used in the equation above is defined as

$$w_A(\mathbf{r}) = \frac{\rho_A^0(\mathbf{r}-\mathbf{r}_A)}{\sum_B \rho_B^0(\mathbf{r}-\mathbf{r}_B)}. \tag{4}$$

Here $\rho_B^0(\mathbf{r})$ is the spherically averaged atomic density for the isolated atom B centered at the origin. It is known that Hirshfeld's method is quite insensitive to the choice of reference density for calculating, say, atomic charges (deProft *et al.*, 2002). The thermally smeared Hirshfeld atom $\langle\rho_A\rangle(\mathbf{r})$ is given by the convolution of ρ_A with a probability distribution function $P_A(\mathbf{r})$ that describes the location of the atom A in space,

$$\langle\rho_A\rangle = \rho_A \star P_A. \tag{5}$$

Here $\star$ represents a convolution. It is these functions $\langle\rho_A\rangle$ for the symmetry-unique atoms in the molecule which are used to obtain the unit-cell density. Where no confusion can arise, we shall also call them 'Hirshfeld atoms'.

2.3. The model for the thermally averaged unit-cell density

The thermally smeared unit-cell density is given as a sum of the thermally smeared atomic densities in the crystal:

$$\begin{aligned}\langle\rho_{\rm cell}\rangle(\mathbf{r}) &= \sum_{C}^{\rm cell}\langle\rho_C\rangle(\mathbf{r}) \\ &= \sum_{a}^{\rm unique\ atoms}\sum_{\{\mathbf{S},\mathbf{t}\}} n_a^{-1}\langle\rho_a\rangle(\mathbf{S}^T(\mathbf{r}-\mathbf{t})).\end{aligned} \tag{6}$$

In the second line, we have used the fact that the unique atoms a are sufficient to generate all atoms C in the unit cell, when acted on by all the crystal symmetry operators. The unique atoms $\{a\}$ constitute an asymmetric unit which is a subset of the atoms $\{A\}$ in the molecule used in the QM calculation described above. The factor n_a, a site-symmetry factor, is the number of times the unique atom a is mapped onto itself (or a lattice transformation of itself) by the crystal symmetry operators $\{\mathbf{S},\mathbf{t}\}$, and is present to avoid double counting.

2.4. Model for the structure factors

The X-ray structure-factor magnitudes F_j^c are calculated by the following model:

$$F_j^c = sX_j(\xi, |F_j|)|F_j|. \tag{7}$$

Here $|F_j|$ is the magnitude of the complex structure factor F_j (discussed below), s is an adjustable overall scale factor and $X_j(\xi, |F_j|)$ accounts for extinction effects, and depends on an empirically adjustable parameter ξ (Larson, 1970). Sometimes multiple scale factors are used for different groups of reflections. This may occur when, for example, reflections are measured with different detector settings or with different crystals, as is often the case in protein crystals where beam damage is common. To account for multiple scale factors, it is only necessary to replace s in equation (7) by $s_{g(j)}$, where $g(j)$ is the index of the group to which the reflection j belongs.

The complex structure factors F_j which appear in the model are directly related to the thermally averaged electron density in the unit cell by a Fourier transform,

$$F_j = \int \langle \rho_{\rm cell} \rangle (\mathbf{r}) \exp(i\mathbf{q}_j \cdot \mathbf{r}) \, {\rm d}\mathbf{r}. \quad (8)$$

Here $\mathbf{q}_j$ is the scattering vector associated with the jth reflection, the difference between the elastically scattered and incident X-ray wavevector

$$\mathbf{q}_j = 2\pi \mathbf{D}^* \mathbf{h}_j \quad (9)$$

with $\mathbf{D}^*$ being the reciprocal-cell matrix and $\mathbf{h}$ the vector of the Miller indices.

Substituting equation (6) in equation (8), we can evaluate the complex structure factors in terms of the Hirshfeld atoms:

$$F_j = \sum_{a}^{\substack{\rm unique \\ \rm atoms}} \sum_{\{\mathbf{S},\mathbf{t}\}} n_a^{-1} \int \langle \rho_a \rangle (\mathbf{S}^T(\mathbf{r} - \mathbf{t})) \exp(i\mathbf{q}_j \cdot \mathbf{r}) \, {\rm d}\mathbf{r}.$$

Now we use the substitution $\mathbf{r}' = \mathbf{S}^T(\mathbf{r} - \mathbf{t})$ or $\mathbf{r} = \mathbf{S}\mathbf{r}' + \mathbf{t}$. Since $\mathbf{S}$ is orthogonal, ${\rm d}\mathbf{r} = {\rm d}\mathbf{r}'$, and we obtain

$$\begin{aligned} F_j &= \sum_{a}^{\substack{\rm unique \\ \rm atoms}} \sum_{\{\mathbf{S},\mathbf{t}\}} n_a^{-1} \int \langle \rho_a \rangle (\mathbf{r}') \exp[i\mathbf{q}_j \cdot (\mathbf{S}\mathbf{r}' + \mathbf{t})] \, {\rm d}\mathbf{r}' \\ &= \sum_{a}^{\substack{\rm unique \\ \rm atoms}} \sum_{\{\mathbf{S},\mathbf{t}\}} n_a^{-1} \exp(i\mathbf{q}_j \cdot \mathbf{t}) \langle f_a \rangle (\mathbf{S}^T \mathbf{q}_j). \end{aligned} \quad (10)$$

In the last line, we have used the definition for the Fourier transform of a (thermally smeared) Hirshfeld atom a,

$$\begin{aligned} \langle f_a \rangle (\mathbf{q}) &= \int \langle \rho_a \rangle (\mathbf{r}) \exp(i\mathbf{q} \cdot \mathbf{r}) \, {\rm d}\mathbf{r} \\ &= \bar{\rho}_a(\mathbf{q}) \exp(i\mathbf{q} \cdot \mathbf{r}_a) \exp(-\mathbf{q}^t \mathbf{U}^a \mathbf{q}/2). \end{aligned} \quad (11)$$

The right-hand side is obtained from equation (5) for atom a. The term $\exp(-\mathbf{q}^T \mathbf{U}^a \mathbf{q}/2)$ is the Fourier transform of probability distribution $P_a(\mathbf{r})$, and the term $\bar{\rho}_a(\mathbf{q})$ is the Fourier transform of the HA centered at the origin, *i.e.* the Fourier synthesis of $\rho_a(\mathbf{r} + \mathbf{r}_a)$,

$$\bar{\rho}_a(\mathbf{q}) = \int \rho_a(\mathbf{r} + \mathbf{r}_a) \exp(i\mathbf{q} \cdot \mathbf{r}) \, {\rm d}\mathbf{r}. \quad (12)$$

If the *rigid-Hirshfeld-atom approximation* is used (discussed below), then $\bar{\rho}_a(\mathbf{q})$ may be regarded as a function of only the atomic positions $\mathbf{r}_a$. Hence $\langle f_a \rangle (\mathbf{q})$, the form factor for the thermally smeared HA, depends only on the atomic position $\mathbf{r}_a$ and the corresponding ADP $\mathbf{U}^a$. The model has therefore been expressed only in terms of the atomic positions and ADPs (as well as the experimental scale factor s and the extinction correction ξ).

It is worth pointing out that equation (11) expresses the thermally smeared aspherical atomic scattering factor only in terms of the ADPs of one atom, despite the fact that the molecular density ρ from which ρ_A is derived involves basis functions centered on pairs of atoms. Hence the thermal smearing scheme used here avoids less elegant partitioning procedures that had to be used previously (Bruning & Feil, 1992; Jayatilaka & Grimwood, 2001).

2.5. Aspherical atomic scattering factors

Evaluation. The evaluation of the Fourier transform of the HAs at the origin, equation (12), is central to the development of this paper, and it is important to specify that we evaluate it using numerical integration techniques developed by Becke for use in quantum chemistry (Becke, 1988). Such methods are straightforward and generally applicable. The atomic partitioning of the molecular density used by Becke is unnecessary since the Hirshfeld technique already generated atomic weight functions w_A which are suitable for this purpose. Otherwise, the integration grids are constructed as a direct product of a radial grid and an angular grid. The exact radial and angular integration grids used are described later.

Atomic charges and moments. Setting $\mathbf{q} = \mathbf{0}$ in the equation above gives the electronic charge of the Hirshfeld atom. Dipole and higher moments of the Hirshfeld atom are also straightforward to obtain using the same numerical integration techniques. Such charges and moments are interesting in their own right (deProft *et al.*, 2002; Krishtal *et al.*, 2006) but are here used to surround an isolated molecule to simulate a crystalline environment.

Computational savings. The *ab initio* calculation of aspherical atomic scattering factors is an expensive procedure. Therefore, it is important to note some computational savings that can be obtained with equation (10).

(i) For certain space groups, a subset of the symmetry operators $\{\mathbf{S}_k, \mathbf{t}_k\}$ may differ from one another only in the translation (glide) part $\mathbf{t}_k$. For such a group of symmetry operators, we can calculate once the common part $n_a^{-1} \langle f_a \rangle (\mathbf{S}_1^T \mathbf{q}_j)$ and multiply it by the sum of the phases $\sum_k \exp(i\mathbf{q}_j \cdot \mathbf{t}_k)$.

(ii) For space groups with the inversion operator, a subset of the symmetry operators $\{\mathbf{S}_k, \mathbf{t}_k\}$ may differ from each other in that $\mathbf{S}_k = -\mathbf{S}_1$, $k > 1$. In this case, $\mathbf{S}_k^T \mathbf{q}_j = -\mathbf{S}_1^T \mathbf{q}_j$ and we can calculate once the common part $n_a^{-1} \langle f_a \rangle (\mathbf{S}_k^T \mathbf{q}_j) = n_a^{-1} \langle f_a \rangle (\mathbf{S}_1^T \mathbf{q}_j)^*$ and multiply it by the sum of the phases $\sum_{k>1} \exp(i\mathbf{q}_j \cdot \mathbf{t}_k)$. [Note that the common part is just the complex conjugate of a term which anyway must be evaluated as part of the contribution $\exp(i\mathbf{q}_j \cdot \mathbf{t}_1) n_a^{-1} \langle f_a \rangle (\mathbf{S}_1^T \mathbf{q}_j)$.]

2.6. The rigid-Hirshfeld-atom approximation

The Hirshfeld weight function w_a and the molecular density ρ both depend explicitly on the coordinates of all the atoms in the molecule chosen for the QM calculation. Hence, the HA

ρ_a also depends explicitly on the coordinates of all those atoms.

For relatively small geometrical changes, it might be expected that ρ_a does not change significantly [this idea is due to Debye (1930)]. Then the geometrical dependence of $\langle f_A \rangle(\mathbf{q})$ is controlled only by the phase factor $\exp(i\mathbf{q} \cdot \mathbf{r}_A)$ in equation (11). In the context of HAs, we shall call Debye's approximation the *rigid-Hirshfeld-atom approximation*. Should this approximation prove to be poor, we can always recalculate the molecular density ρ, the Hirshfeld atom ρ_a, and hence the aspherical atomic scattering factors for atom a. Any physical quantities such as atom positions and ADPs that have been derived using this rigid-Hirshfeld-atom assumption can then be redetermined with the recalculated aspherical atomic scattering factors. Thus the rigid approximation can be removed by an iterative process if necessary.

The importance of the rigid HA model lies in the fact that the aspherical atomic scattering factors are much more efficiently calculated using this approximation: a change in the positional parameters of the atom a by $\Delta\mathbf{r}_a$ merely multiplies the $\langle f_A \rangle(\mathbf{q})$ by the phase factor $\exp(i\mathbf{q} \cdot \Delta\mathbf{r}_a)$. Use of this fact avoids an expensive QM calculation for ρ and a computationally expensive numerical integration.

2.7. Refinement of model parameters

The least-squares refinement for the crystal structure parameters is obtained by minimizing the agreement statistic

$$\chi^2 = \frac{1}{N_r - N_p} \sum_j \frac{(F_j^c - F_j^e)^2}{\sigma_j^2}. \qquad (13)$$

This statistic depends on the experimental structure factors and errors, the number of reflections N_r, and the number of parameters N_p in the model. We have implemented a conjugate-gradient-minimization procedure as well as a standard normal-equations approach to obtain the structural parameters (Press *et al.*, 1992) and we have found the latter to be completely adequate for the cases examined here. The details of these minimization techniques are well known in crystallography (Coppens, 1997) (the derivative expressions required to implement such methods can also be derived from the preceding details). We shall not discuss those methods here, except to note some key points of the implementation.

(i) Unlike other crystallographic programs, the minimization is performed in Cartesian rather than fractional coordinates. The reason for this is that the aspherical atomic scattering factors are not tabulated but are most easily calculated directly in the Cartesian frame used for the QM calculation.

(ii) Because of the use of Cartesian coordinates, some of the parameters may be redundant due to symmetry constraints. To enforce symmetry, we use projection operators; and to eliminate symmetry-redundant coordinates we use the eigenvalue filtering technique proposed by Diamond (1966), which has the advantage that any combination of parameters which is poorly defined is also removed from the refinement without difficulty.

(iii) From a starting structure, a QM calculation is performed and the rigid-Hirshfeld-atom approximation is applied. The least-squares equations are solved to obtain a provisional crystal structure. This structure may then be used in another QM calculation and another structure refinement to test whether the rigid approximation is acceptable.

Finally, the required QM calculations and the refinement process have been coded in the program *Tonto* (Jayatilaka & Grimwood, 2003) which is available free of charge under the GNU-public license from the sourceforge repository (http://sourceforge.net/projects/tonto).

3. The examples of benzene and urea

In this section, we describe the application of the method to benzene and urea crystals.

3.1. Details of the experimental data and refinement

It is important to have an independent determination of the geometrical parameters to which our refined crystal structure parameters can be compared. For both benzene and urea, neutron diffraction experiments provide this benchmark. Neutron diffraction has been chosen because neutrons scatter directly from the nuclei and in addition the scattering from hydrogen nuclei is strong relative to the other nuclei, unlike X-ray diffraction where the scattering from the H atoms is weak.

For both benzene (Jeffrey *et al.*, 1987) and urea (Swaminathan *et al.*, 1984), 123 K neutron diffraction results including ADPs of all atoms as well as reliable X-ray diffraction data (Bürgi *et al.*, 2002; Birkedal *et al.*, 2004) are available. For benzene, a multi-temperature analysis of an $AgClO_4$–benzene complex (McMullan *et al.*, 1997) established the temperature dependence of the D-atom ADPs and allowed scaling of these neutron data – taking into account isotope effects – to the temperature of the X-ray experiment, which was found to be 110 K (Bürgi *et al.*, 2002). For urea, high-resolution synchrotron data (Birkedal *et al.*, 2004) were measured at 123 K, the temperature of the neutron experiment. Hence carefully determined neutron ADPs are available, matching the temperature of the X-ray experiments for both compounds. The X-ray geometry provided the starting geometry for all atoms including H for both compounds. It was attempted to start the refinement process from the neutron geometries, leading to the same result. In addition, for urea the starting parameters for a few atoms were changed from the X-ray result and the same refined result was again obtained. For benzene, a cut-off of 4σ on F was used leading to 1766 reflections. For urea, all reflections were included as in the original paper. It was not necessary to include an extinction parameter in the models.

3.2. Details of the quantum-mechanical calculations

In the quantum-mechanical calculations, the cc-pVDZ and cc-pVTZ Gaussian basis sets were used (Dunning, 1989) to

Table 1
Figures of merit (R factors in %) for Hirshfeld-atom structure refinements for different basis sets compared with those for the multipole model.

Results for the multipole model were taken from the literature.

	Multipole model	Hirshfeld-atom refinement		
		HF/cc-pVDZ	HF/cc-pVTZ	HF/cc-pVQZ
Benzene				
$R(F)$	1.89	2.17	2.16	2.16
$R_w(F)$	1.68	2.11	2.08	2.08
$R(F^2)$	2.27	3.08	3.07	3.08
$R_w(F^2)$	3.60	3.35	3.29	3.29
χ^2	–	1.64	1.59	1.59
S	1.04	1.28	1.26	1.26
Urea				
$R(F)$	2.02	1.71	1.66	1.66
$R_w(F)$	0.54	1.27	1.21	1.21
$R(F^2)$	0.71	2.30	2.23	2.22
$R_w(F^2)$	1.08	1.82	1.69	1.69
χ^2	–	9.40	8.51	8.53
S	1.17	3.07	2.92	2.92

Table 2
Figures of merit (R factors in %) for Hirshfeld-atom refinement for benzene and urea with and without a surrounding cluster of point charges.

	HF/cc-pVTZ	HF/cc-pVTZ+− (cluster of charges)
Benzene		
$R_1(F)$	2.16	2.16
$R_w(F)$	2.08	2.09
$R(F^2)$	3.07	3.06
$R_w(F^2)$	3.29	3.33
χ^2	1.59	1.60
GoF	1.26	1.27
Urea		
$R_1(F)$	1.67	1.54
$R_w(F)$	1.22	1.11
$R(F^2)$	2.25	2.17
$R_w(F^2)$	1.69	1.91
χ^2	8.35	7.14
GoF	2.89	2.67

Table 3
Figures of merit (R factors in %) for Hirshfeld-atom structure refinements for the BLYP level of theory for benzene and urea; the final column includes a surrounding cluster of charges.

	Hirshfeld-atom refinement			
	BLYP/cc-pVDZ	BLYP/cc-pVTZ	BLYP/cc-pVQZ	BLYP/cc-pVQZ+−
Benzene				
$R(F)$	2.16	2.15	2.15	2.15
$R_w(F)$	2.09	2.07	2.07	2.08
$R(F^2)$	3.17	3.44	3.46	3.45
$R_w(F^2)$	3.35	3.53	3.55	3.61
χ^2	1.60	1.57	1.57	1.59
S	1.27	1.25	1.25	1.26
Urea				
$R(F)$	1.57	1.53	1.54	1.40
$R_w(F)$	1.10	1.08	1.10	0.88
$R(F^2)$	1.96	1.87	1.88	1.67
$R_w(F^2)$	1.46	1.45	1.47	1.07
χ^2	7.04	6.82	7.04	4.51
S	2.65	2.61	2.65	2.12

Table 4
Bond distances (Å) from neutron diffraction and Hartree–Fock Hirshfeld-atom (HA) refinement for benzene and urea using BLYP theory with surrounding cluster of point charges; differences Δ between them multiplied by 1000.

Bond	Neutron	HA (cc-pVDZ)	Δ	HA (cc-pVTZ)	Δ
Benzene					
C1—C2	1.3943 (11)	1.3954 (4)	1.1	1.3957 (4)	1.4
C2—C3	1.3954 (11)	1.3958 (4)	0.4	1.3961 (4)	0.7
C1—C3a	1.3922 (11)	1.3944 (3)	2.2	1.3947 (3)	2.5
C1—H1	1.084 (2)	1.078 (5)	−6.0	1.081 (5)	−3.0
C2—H2	1.085 (2)	1.086 (5)	1.0	1.088 (5)	3.0
C3—H3	1.083 (2)	1.073 (5)	−10.0	1.076 (5)	−7.0
Urea					
O1—C1	1.258 (1)	1.2557 (4)	0.0	1.2560 (4)	2.0
N1—H2	1.000 (2)	0.987 (5)	−13.0	0.991 (5)	−9.0
N1—C1	1.341 (1)	1.3412 (3)	0.0	1.3413 (2)	0.0
N1—H1	1.007 (2)	1.024 (3)	16.0	1.026 (3)	18.0

expand the molecular orbitals. Both Hartree–Fock and BLYP density functional calculations were used.

In performing the numerical integrations to obtain the aspherical atomic scattering factors, a scheme similar to the one developed by Becke was used (Becke, 1988). The radial grid used was the 'Log 3' grid described by Mura & Knowles (1996) with an equal spacing of radial points before the Log 3 remapping. 35 radial integration points were used for the H atom with 5 extra points per n shell for the heavier atoms. We used angular quadrature grids developed by Lebedev and Laikov. The order of the angular grid was $L = 35$ for non-H atoms and $L = 29$ for the H atoms, and in addition the angular pruning scheme of Treutler & Ahlrichs (1995) was used to make the angular grids smaller nearer the nucleus.

Some of the quantum-mechanical calculations described below introduce a cluster of charges around the isolated molecule to simulate the effect of the crystal environment. These charges were calculated from the Hirshfeld atoms (§2.2) and they were placed at the positions of the atoms in the surrounding molecules. Only those molecules with an atom within a radius of 5 Å of the central molecule were included. In addition, atomic dipoles for the Hirshfeld atoms were calculated, and two charges were placed at the positions of the atoms (actually at a distance ±0.001 a.u. from the atomic position) in the surrounding molecules in such a way as to simulate the atomic dipole moment of the Hirshfeld atom. The Hartree–Fock or BLYP calculation was then repeated in the presence of these charges, and new atomic charges were calculated and propagated to the surrounding molecules. The quantum-mechanical calculations were repeated, propagating these charges, until the results ceased to change.

3.3. Comparison with multipole refinement and the effect of basis set

Starting from the neutron diffraction crystal structures, the Hirshfeld-atom refinement technique was applied by solving the normal equations. All positions and ADPs were refined.

Table 5
Anisotropic displacement parameters (ADPs) (/10^4 Å^2) for benzene from neutron diffraction at 123 K and from D-atom ADPs scaled *via* multi-temperature analysis (MTA), compared to Hirshfeld-atom refinement results using Hartree–Fock (HF) and BLYP theory for several basis sets.

Calculations which include a surrounding cluster of charges are indicated by postfixed +−.

Method	Atom	U_{11}	U_{22}	U_{33}	U_{12}	U_{13}	U_{23}
Neutron	C1	232 (3)	200 (3)	262 (3)	17 (3)	−13 (3)	−12 (3)
MTA		211	186	238	13	−7	−9
HF/cc-pVDZ		216.9 (8)	194.2 (7)	247.7 (8)	13.7 (7)	−9.0 (8)	−8.7 (7)
HF/cc-pVTZ		217.0 (8)	194.0 (7)	247.9 (8)	14.3 (7)	−7.3 (8)	−8.0 (7)
HF/cc-pVTZ+−		217.2 (8)	194.0 (7)	248.1 (8)	14.4 (7)	−7.3 (8)	−8.0 (7)
BLYP/cc-pVTZ		214.6 (8)	192.5 (7)	245.9 (8)	13.0 (7)	−12.0 (8)	−9.8 (7)
BLYP/cc-pVTZ+−		212.9 (8)	190.6 (7)	244.0 (8)	13.6 (7)	−10.0 (8)	−9.0 (7)
Neutron	C2	218 (3)	255 (3)	242 (3)	14 (3)	33 (3)	−16 (3)
MTA		195	236	222	13	27	−17
HF/cc-pVDZ		199.5 (8)	245.5 (8)	231.4 (8)	13.8 (7)	26.3 (8)	−16.8 (8)
HF/cc-pVTZ		200.0 (8)	244.7 (9)	231.9 (8)	14.5 (7)	28.1 (8)	−15.9 (8)
HF/cc-pVTZ+−		200.1 (8)	244.9 (9)	232.0 (8)	14.7 (7)	28.5 (8)	−15.9 (8)
BLYP/cc-pVTZ		196.5 (8)	245.2 (9)	228.8 (8)	12.7 (7)	24.1 (8)	−18.4 (8)
BLYP/cc-pVTZ+−		195.3 (8)	242.4 (9)	227.5 (8)	13.3 (7)	26.0 (8)	−17.8 (8)
Neutron	C3	230 (3)	237 (3)	233 (3)	−22 (3)	17 (3)	19 (3)
MTA		206	215	217	−17	11	18
HF/cc-pVDZ		211.3 (8)	225.6 (8)	225.9 (8)	−17.6 (7)	10.1 (8)	19.4 (8)
HF/cc-pVTZ		211.5 (8)	225.3 (8)	226.3 (8)	−16.7 (7)	11.6 (8)	19.6 (8)
HF/cc-pVTZ+−		211.7 (8)	225.3 (8)	226.4 (8)	−16.7 (7)	11.8 (8)	19.8 (8)
BLYP/cc-pVTZ		209.3 (8)	224.6 (8)	223.3 (8)	−19.2 (7)	7.6 (8)	19.1 (8)
BLYP/cc-pVTZ+−		208.0 (8)	222.1 (8)	221.7 (8)	−18.1 (7)	9.2 (8)	19.2 (8)
Neutron	H1	472 (5)	262 (3)	519 (6)	83 (3)	2 (5)	−2 (4)
MTA		478	260	533	85	18	8
HF/cc-pVDZ		490 (30)	400 (30)	500 (30)	10 (20)	0 (20)	30 (20)
HF/cc-pVTZ		530 (30)	390 (30)	520 (30)	20 (20)	10 (20)	40 (20)
HF/cc-pVTZ+−		530 (30)	380 (30)	520 (30)	30 (20)	0 (20)	40 (20)
BLYP/cc-pVTZ		480 (30)	330 (20)	520 (30)	60 (20)	−10 (20)	30 (20)
BLYP/cc-pVTZ+−		490 (30)	320 (20)	490 (30)	60 (20)	0 (20)	40 (20)
Neutron	H2	400 (5)	469 (5)	449 (5)	69 (4)	168 (5)	−32 (5)
MTA		403	489	458	81	177	−34
HF/cc-pVDZ		450 (30)	450 (30)	560 (30)	60 (20)	140 (30)	20 (30)
HF/cc-pVTZ		470 (30)	470 (30)	580 (30)	70 (20)	150 (30)	20 (30)
HF/cc-pVTZ+−		460 (30)	470 (30)	570 (30)	80 (20)	160 (30)	20 (30)
BLYP/cc-pVTZ		410 (30)	460 (30)	520 (30)	70 (20)	160 (20)	10 (20)
BLYP/cc-pVTZ+−		400 (30)	460 (30)	500 (30)	80 (20)	160 (20)	0 (20)
Neutron	H3	450 (5)	400 (5)	428 (5)	−63 (4)	91 (5)	124 (4)
MTA		471	398	433	−58	104	125
HF/cc-pVDZ		470 (30)	460 (30)	500 (30)	30 (20)	10 (30)	20 (30)
HF/cc-pVTZ		500 (30)	480 (30)	520 (30)	20 (20)	20 (30)	40 (30)
HF/cc-pVTZ+−		500 (30)	470 (30)	510 (30)	10 (20)	20 (30)	40 (30)
BLYP/cc-pVTZ		470 (30)	430 (30)	460 (30)	0 (20)	60 (20)	80 (20)
BLYP/cc-pVTZ+−		490 (30)	410 (30)	470 (30)	0 (20)	50 (20)	90 (20)

Table 1 gives the various figures of merit obtained using Hirshfeld-atom refinement using Hartree–Fock calculations with different basis sets. It can be seen that the Hirshfeld-atom model yields slightly worse figures of merit than the multipole model. This is perhaps not surprising since the multipole refinement is based on adjusting a large number of charge-density population parameters to the X-ray data, while the Hirshfeld-atom refinement uses fixed electron-density fragments derived from theory. Still, the fact that the Hirshfeld-atom refinement almost reproduces the experimental result is very encouraging, and it supports earlier findings where invariom density fragments were used (Dittrich *et al.*, 2007). A more detailed comparison between this and the invariom approach will be the topic of a subsequent study.

Table 1 shows that the double-ζ cc-pVTZ basis is already sufficiently converged with respect to the figures of merit. There is no improvement from the cc-pVQZ basis in terms of R factor and goodness of fit.

3.4. The effect of the crystal environment

To simulate the effect of the crystal field, we have undertaken calculations with surrounding point charges derived from Hirshfeld partitioning of the molecular density, as

Table 6
Anisotropic displacement parameters (ADPs) (/10^4 Å^2) for urea from neutron diffraction (at 123 K) scaled to fit the X-ray data, compared to Hirshfeld-atom refinement results using Hartree–Fock (HF) and BLYP theories for several basis sets.

Calculations which include a surrounding cluster of charges are indicated by postfixed +−.

Method	Atom	U_{11}	U_{22}	U_{33}	U_{12}	U_{13}	U_{23}
Neutron	O1	197 (6)	197 (6)	63 (4)	17 (5)	0	0
HF/cc-pVDZ		192.7 (7)	192.7 (7)	66.3 (6)	13 (1)	0.0 (0)	0.0 (0)
HF/cc-pVTZ		194.1 (7)	194.1 (7)	66.1 (6)	13 (1)	0.0 (0)	0.0 (0)
HF/cc-pVTZ+−		193.8 (6)	193.8 (6)	66.6 (5)	15 (1)	0.0 (0)	0.0 (0)
BLYP/cc-pVTZ		193.9 (6)	193.9 (6)	64.6 (5)	16 (1)	0.0 (0)	0.0 (0)
BLYP/cc-pVTZ+−		193.5 (5)	193.5 (5)	65.2 (4)	17.4 (8)	0.0 (0)	0.0 (0)
Neutron	N1	286 (4)	286 (4)	95 (2)	−147 (2)	2 (3)	2 (3)
HF/cc-pVDZ		283.6 (9)	283.6 (9)	97.0 (6)	−145 (1)	1.1 (5)	1.1 (5)
HF/cc-pVTZ		285.9 (8)	285.9 (8)	96.7 (6)	−147 (1)	1.2 (5)	1.2 (5)
HF/cc-pVTZ+−		286.3 (7)	286.3 (7)	95.2 (5)	−148 (1)	0.7 (5)	0.7 (5)
BLYP/cc-pVTZ		288.3 (8)	288.3 (8)	94.6 (4)	−149 (1)	1.1 (5)	1.1 (5)
BLYP/cc-pVTZ+−		288.3 (6)	288.3 (6)	93.5 (4)	−150.4 (8)	0.5 (4)	0.5 (4)
Neutron	C1	147 (5)	147 (5)	65 (3)	1 (4)	0	0
HF/cc-pVDZ		147.9 (7)	147.9 (7)	65.6 (7)	−3 (1)	0.0 (0)	0.0 (0)
HF/cc-pVTZ		148.9 (7)	148.9 (7)	65.3 (7)	−4 (1)	0.0 (0)	0.0 (0)
HF/cc-pVTZ+−		148.6 (6)	148.6 (6)	65.8 (6)	−5 (1)	0.0 (0)	0.0 (0)
BLYP/cc-pVTZ		146.0 (6)	146.0 (6)	65.7 (6)	1 (1)	0.0 (0)	0.0 (0)
BLYP/cc-pVTZ+−		145.8 (5)	145.8 (5)	66.1 (5)	0.7 (8)	0.0 (0)	0.0 (0)
Neutron	H1	440 (11)	440 (11)	216 (7)	−222 (8)	−31 (9)	−31 (9)
HF/cc-pVDZ		740 (40)	740 (40)	200 (30)	−420 (40)	−130 (20)	−130 (20)
HF/cc-pVTZ		750 (30)	750 (30)	230 (30)	−410 (40)	−130 (20)	−130 (20)
HF/cc-pVTZ+−		620 (30)	620 (30)	260 (30)	−360 (30)	−120 (20)	−120 (20)
BLYP/cc-pVTZ		660 (30)	660 (30)	140 (30)	−400 (30)	0 (20)	0 (20)
BLYP/cc-pVTZ+−		550 (20)	550 (20)	170 (20)	−350 (30)	0 (10)	0 (10)
Neutron	H2	430 (10)	430 (10)	140 (6)	−158 (8)	19 (8)	19 (8)
HF/cc-pVDZ		520 (20)	520 (20)	280 (30)	−10 (40)	30 (20)	30 (20)
HF/cc-pVTZ		540 (20)	540 (20)	290 (30)	−90 (40)	20 (20)	20 (20)
HF/cc-pVTZ+−		530 (20)	530 (20)	190 (20)	−120 (40)	−20 (20)	−20 (20)
BLYP/cc-pVTZ		450 (20)	450 (20)	360 (30)	−180 (30)	−20 (20)	−20 (20)
BLYP/cc-pVTZ+−		450 (20)	450 (20)	260 (20)	−190 (30)	−20 (10)	−20 (10)

described above. The simulation of such effects by point charges and dipoles might be insufficient, *e.g.* for situations with strong hydrogen bonding. A more exhaustive treatment will be the subject of future work. The radius of the surrounding cluster used here was 5 Å. Table 2 shows the agreement statistics. For urea, for the cluster-of-charges model, the agreement is systematically better than when isolated molecules are used. However, for benzene where there are no strong intermolecular interactions apart from the C—H$\cdots\pi$ interaction, there is no obvious improvement.

3.5. The effect of electron correlation

Table 3 shows that including electron correlation by performing the calculations on the BLYP level of theory does improve R factors and can also still be detected in the goodness of fit and χ^2 for hydrogen-bonded urea, while for benzene the improvements are insignificant. We can also see that changing the basis set does not improve the results much after cc-pVTZ. Hence, including a surrounding cluster of charges is more important than using a large basis set. The best possible fit is achieved when combining the BLYP level of theory with a surrounding cluster of charges.

3.6. Bond lengths obtained

Table 4 lists the geometries for benzene and urea together with the results of the Hirshfeld-atom refinement. In benzene, there is an inversion center in the mid-point of each ring, resulting in three unique C atoms and three unique H atoms. For urea, the atoms sit on special positions and the whole molecule can be generated by the asymmetric unit consisting of only half the number of atoms.

From Table 4, we see that non-hydrogen-bond lengths are within 0.002 Å of the neutron diffraction results and hydrogen-bond lengths are within 0.01 Å except for one which is within 0.02 Å. We do not see a pronounced effect of the basis set on the geometry. The geometry from neutron and X-ray diffraction agrees well also for the H atoms. The cc-pVDZ basis seems already sufficient to model the most dominant aspherical features of the electron density. An influence of larger basis sets might be expected when even higher data resolutions were available. One can conclude that the cc-pVDZ basis already provides an improved density description over the multipole model and is sufficient for investigating the geometry of larger molecules when basis-set size might become a limiting factor.

3.7. Anisotropic displacement parameters (ADPs)

A result of this work which is of special interest to the crystallographic community is that H-atom ADPs can be directly refined from the X-ray data (see below). So far, the consensus among crystallographers is that H-atom ADPs cannot be obtained from single-crystal X-ray diffraction data (Hirshfeld, 1976). This is undoubtedly the case when using the independent-atom model and also when we determine the electron density in a multipole refinement, as electron density and thermal motion are convoluted and therefore intimately related. However, in cases when the electron-density distribution is known *a priori* (Dittrich *et al.*, 2005), like the approach taken in this paper where the electron density is calculated from high-level quantum chemistry, the thermal motion of H atoms becomes accessible by experiment, as the contamination of ADPs due to bonding electron density that occurs when using the independent-atom model (Hummel, Raselli & Bürgi, 1990) is expected to be absent. Earlier preliminary results using the multipole model did not justify early optimism and the ADPs from the invariom database (Dittrich *et al.*, 2006) still showed systematic differences, mostly with atoms that were involved in hydrogen bonding, *i.e.* the surrounding molecules. The conclusion at the time was that differences in the refined ADPs were due to the influence of hydrogen bonding or, more generally, the surrounding molecules. A possible solution to this problem that is also applicable to larger molecules where a SCF calculation can be afforded is to include the charges of the cluster of molecules surrounding a molecule.

Now to the results of this work. Table 5 lists the neutron ADPs for benzene together with the results of a multi-temperature study (Bürgi *et al.*, 2002) that provide reference values for comparison. The Hirshfeld-atom refinement results were calculated on the Hartree–Fock level of theory for two basis sets and also included cluster charges. As expected, differences in the C-atom ADPs are rather small for benzene. Interestingly, the C-atom ADPs for the Hirshfeld-atom fit lie in between the neutron and the multi-temperature results.

While the ADPs of the C atoms do not change much with the size of the basis set, H-atom ADPs do show a more pronounced basis-set dependence. While H1 and H2 atoms are reduced with increasing basis-set size, the H3 atom shows the opposite trend. We suppose that a more extended basis set with diffuse electron density might correlate with the atomic displacement parameters. A very interesting result is that H-atom ADPs improve when the BLYP level of theory is employed and show the closest agreement with the multi-temperature results. When reflecting on the small changes of the *R* factor reported earlier, these quite considerable improvements in the ADPs that leave the figures of merit almost unchanged lead us to the conclusion that the *R* factor is rather too insensitive to highlight improvements at this level of detail.

Table 6 lists the neutron ADPs for urea together with the results of the Hirshfeld-atom refinement, the results from neutron diffraction and the result where cluster charges were included. For urea, ADPs again improve substantially when using a cluster of point charges to surround the molecule and when using the BLYP level of theory to model electron correlation. To highlight what contribution is due to electron correlation and what due to the cluster charges, we have also added the results for BLYP/cc-pVTZ, showing that the former dominates. However, significant differences remain.

The possibility that these differences in the ADPs are due to an inadequate electron-density model (one which does not include the perturbing effects of nearby molecules, or which does not include electron correlation effects) can most likely be ruled out. However, two caveats should be noted. (i) The use of point charges to simulate the crystal field does not allow for electron exchange effects, and (ii) the use of BLYP theory to treat electron correlation effects is not ideal for the intermolecular hydrogen bonds in urea.

The differences in the ADPs may also be due to systematic error in either the experimental X-ray or neutron data. Blessing (1995) has discussed possible reasons for such differences.

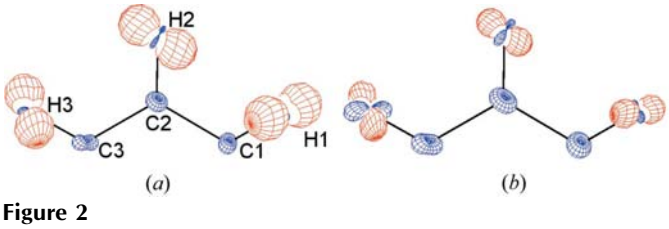

Figure 2
Differences between ADPs refined from neutron minus Hirshfeld-atom refinement as displayed with the program *peanut* (Hummel, Hauser & Bürgi, 1990) for benzene (only the asymmetric unit is shown). A scale of 6.15 for the RMSD surfaces has been used. (*a*) shows the difference neutron − HF/cc-pVTZ+−, (*b*) shows the difference neutron − BLYP/cc-pVTZ+−. A reduction of the differences for the BLYP (*b*) compared to the HF level of theory (*a*) can be seen.

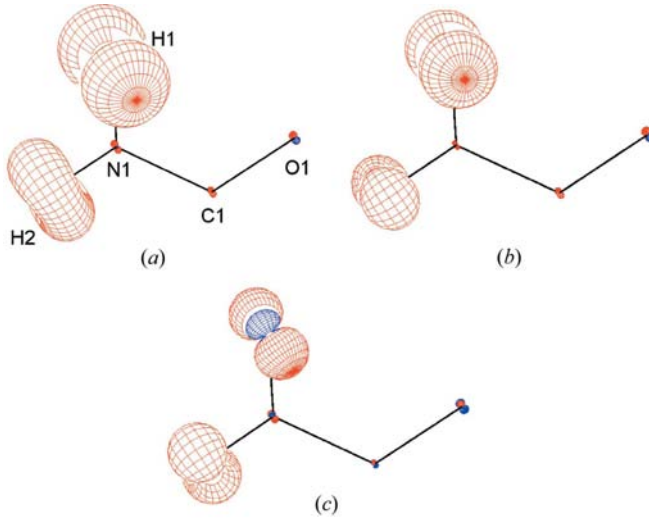

Figure 3
Differences between ADPs refined from neutron minus Hirshfeld-atom refinement as displayed with the program *peanut* (Hummel, Hauser & Bürgi, 1990) for urea showing only the asymmetric unit. A scale of 6.15 for the RMSD surfaces has been used. (*a*) shows the difference neutron − HF/cc-pVTZ, (*b*) shows the difference neutron − HF/cc-pVTZ+− and (*c*) shows neutron − BLYP/cc-pVTZ+−.

One likely systematic error that might still be contained in the X-ray data is thermal diffuse scattering. An analysis of low-temperature or multi-temperature data might be helpful to test this possibility, as a better agreement between X-ray and neutron ADP results has been reported at temperatures around 20 K (Iversen *et al.*, 1996). It cannot be ruled out that the neutron data are also affected by extinction and absorption problems, which will be smaller or absent for the X-ray data due to crystal size.

Differences in ADPs are easier to analyse and become more obvious when visualized. Figs. 2 and 3 show differences between neutron and Hirshfeld-atom refinement results in terms of root mean square displacements (RMSDs) using the program *peanut* (Hummel, Hauser & Bürgi, 1990) for benzene and urea. The first observation that can be made is that, for benzene, heavy-atom ADPs from Hirshfeld-atom refinement are systematically smaller than for the neutron data, although differences are small. For urea, no obvious contamination of bonding electron density occurs for the non-H atoms as differences are small and randomly distributed. For benzene, the difference calculated from the neutron ADPs minus their Hirshfeld-atom refinement counterparts is reduced when the BLYP method is used (Fig. 2*b*) compared to the HF result (Fig. 2*a*), especially for the H atoms, although H-atom ADPs are still overestimated in the Hirshfeld-atom refinement. For urea, the isolated-molecule scattering factors are expected to result in inferior H-atom ADPs, as the effects of hydrogen bonding are not included in the model density. That is supported by comparison with the neutron result using the basis HF/cc-pVTZ (Fig. 3*a*). The agreement is improved by including the cluster charges for the same basis (Fig. 3*b*) and is best for the combination BLYP/cc-pVTZ and cluster charges (Fig. 3*c*).

3.8. Contribution of the H-atom ADPs to the figures of merit

To establish whether the experimental data are accurate enough to determine the H-atom ADPs, we have calculated and compared two sets of structure factors: those with the H-atom ADPs fixed, and those with the H atoms refined. The agreement statistics show that the difference is observable in the χ^2 agreement statistic (1.79 with fixed H-atom ADPs, 1.63 for adjusted ones), however the effect is only of the order of 0.05% in the R factor.

3.9. Computational time of the refinement and the use of the conjugate gradient method

Most of the computational time using the approach was taken by (i) the initial SCF required to obtain the molecular density, and (ii) the time taken to calculate the aspherical scattering factors. After the latter are available, of the order of ten iterations are required to obtain the refined structure using the normal-equations method, and this part of the calculation proceeds in much less than one second on a normal personal computer.

We have also implemented a refinement procedure based on the Broyden–Fletcher–Goldfarb–Shanno (BFGS) conjugate-gradient minimization of the least-squares function. The results obtained were the same as those obtained from least-squares minimization, except that more steps were required to obtain the refined structure. It is recommended to use the normal-equation method for structure refinement with Hirshfeld atoms.

4. Conclusions

A new approach to crystal structure refinement has been described. Specifically, aspherical atomic density functions (ADFs) are obtained by partitioning a quantum-mechanical electron density using Hirshfeld's method. The positions of these ADFs, and their atomic displacement parameters, are adjusted to fit the measured X-ray diffraction data by minimizing the least-squares error. The method has been successfully applied to the case of benzene and urea. The following conclusions may be drawn.

(i) The refined structure obtained from the Hirshfeld-atom method has figures of merit close to those obtained from a multipole refinement with very many fewer adjustable parameters.

(ii) The structure factors calculated using the Hirshfeld-atom method are better than those obtained by partitioning the ADPs between two atomic centers, as used previously. The Hirshfeld-atom method is more elegant and is recommended for structure-factor calculation.

(iii) The refined geometrical parameters, even those for H atoms, are very close to those observed from neutron diffraction experiments: non-hydrogen bond lengths are within 0.002 Å while hydrogen bond lengths are mostly within 0.01 Å.

(iv) The ADPs for heavy atoms are very close to those obtained from neutron experiments, while those for H atoms are larger by about 20% compared to corresponding neutron diffraction ADPs.

(v) Calculations that include electron correlation and that simulate the effect of the crystal environment using point charges lead to an improvement in the H-atom ADPs relative to the neutron diffraction results. The best agreement can be achieved with the BLYP level of theory in combination with cluster charges.

(vi) The time for the refinement procedure is dominated by the quantum-mechanical calculation time and also the time to calculate the aspherical atomic scattering factors. A negligible time is required for the actual structure refinement.

We thank D. Grimwood for contributing to the ADP refinement procedure and C. B. Hübschle for help with converting ADP differences from cif into scfs file format. Thanks to A. Volkov for notifying us of the angular integration grid code of D. Laikov and C. van Wüllen. Access to the X-ray data for benzene from H.-B. Bürgi is also acknowledged. This work was supported by the Deutsche Forschungsgemeinschaft DFG (DI 921/3-1) and the Australian Synchrotron Research Program (ASRP), which is funded by the Commonwealth of Australia under the Major National

Research Facilities Program. The *Tonto* program has been developed with funding from the Australian Research Council.

References

Becke, A. D. (1988). *J. Chem. Phys.* **88**, 2547.
Birkedal, H., Madsen, D., Mathiesen, R. H., Knudsen, K., Weber, H.-P., Pattison, P. & Schwarzenbach, D. (2004). *Acta Cryst.* A**60**, 371–381.
Blessing, R. H. (1995). *Acta Cryst.* B**51**, 816–823.
Bruning, H. & Feil, D. (1992). *Acta Cryst.* A**48**, 865–872.
Bürgi, H. B., Capelli, S. C., Goeta, A. E., Howard, J. A. K., Spackman, M. A. & Yufit, D. S. (2002). *Chem. Eur. J.* **8**, 3512–3521.
Bytheway, I., Chandler, G., Figgis, B. & Jayatilaka, D. (2007). *Acta Cryst.* A**63**, 135–145.
Clementi, E. & Roetti, C. (1974). *At. Data Nucl. Data Tables*, **14**, 177–478.
Coppens, P. (1997). *X-Ray Charge Densities and Chemical Bonding. IUCr Texts on Crystallography*, No. 4. Oxford University Press/ IUCr.
Coppens, P. (2005). *Angew. Chem. Int. Ed.* **44**, 6810–6811.
Debye, P. (1930). *Z. Phys.* **31**, 419.
Destro, R. & Merati, F. (1995). *Acta Cryst.* B**51**, 559–570.
Diamond, R. (1966). *Acta Cryst.* **21**, 253–266.
Dittrich, B., Hübschle, C. B., Luger, P. & Spackman, M. A. (2006). *Acta Cryst.* D**62**, 1325–1335.
Dittrich, B., Koritsánszky, T. & Luger, P. (2004). *Angew. Chem. Int. Ed.* **43**, 2718–2721.
Dittrich, B., Munshi, P. & Spackman, M. A. (2007). *Acta Cryst.* B**63**, 505–509.
Dittrich, B., Whitten, A. & Spackman, M. A. (2005). *Acta Cryst.* A**61**, C420.
Dominiak, P. M., Volkov, A., Li, X., Messerschmidt, M. & Coppens, P. (2007). *J. Chem. Theory Comput.* **2**, 232–247.
Dunning, T. H. (1989). *J. Chem. Phys.* **90**, 1007–1023.
Grimwood, D. J., Bytheway, I. & Jayatilaka, D. (2003). *J. Comput. Chem.* **24**, 470–483.
Grimwood, D. J. & Jayatilaka, D. (2001). *Acta Cryst.* A**57**, 87–100.
Hansen, N. K. & Coppens, P. (1978). *Acta Cryst.* A**34**, 909–921.
Hirshfeld, F. L. (1976). *Acta Cryst.* A**32**, 239–244.
Hirshfeld, F. L. (1977). *Theor. Chim. Acta*, **44**, 129–138.
Hummel, W., Hauser, J. & Bürgi, H.-B. (1990). *J. Mol. Graphics*, **8**, 214–218.
Hummel, W., Raselli, A. & Bürgi, H.-B. (1990). *Acta Cryst.* B**46**, 683–692.
Iversen, B. B., Larsen, F. K., Figgis, B. N., Reynolds, P. A. & Schultz, A. J. (1996). *Acta Cryst.* B**52**, 923–931.
Jayatilaka, D. (1998). *Phys. Rev. Lett.* **80**, 798–801.
Jayatilaka, D. & Grimwood, D. J. (2001). *Acta Cryst.* A**57**, 76–86.
Jayatilaka, D. & Grimwood, D. J. (2003). *Comput. Sci. ICCS 2003*, **2660**, 142–151.
Jeffrey, G. A., Ruble, J. R., McMullan, R. K. & Pople, J. A. (1987). *Proc. R. Soc. London*, **414**, 47–57.
Koritsánszky, T. & Volkov, A. (2004). *Chem. Phys. Lett.* **385**, 431–434.
Koritsanszky, T., Volkov, A. & Coppens, P. (2002). *Acta Cryst.* A**58**, 464–472.
Krishtal, A., Senet, P., Yang, M. & Alsenoy, C. V. (2006). *J. Chem. Phys.* **125**, 34312.
Larson, A. C. (1970). *Crystallographic Computing*, edited by F. R. Ahmed, pp. 291–294. Copenhagen: Munksgaard.
McMullan, R. K., Koetzle, T. F. & Fritchie, C. J. (1997). *Acta Cryst.* B**53**, 645–653.
Madsen, A. Ø, Sørensen, H. O., Flensburg, C., Stewart, R. F. & Larsen, S. (2004). *Acta Cryst.* A**60**, 550–561.
Mura, M. E. & Knowles, P. J. (1996). *J. Chem. Phys.* **104**, 9848–9858.
Pichon-Pesme, V., Lecomte, C. & Lachekar, H. (1995). *J. Phys. Chem.* **99**, 6242–6250.
Press, W. H., Teukolsky, S. A., Vetterling, W. T. & Flannery, B. P. (1992). *Numerical Recipes in Fortran – The Art of Scientific Computing*, 2nd ed. Cambridge University Press.
deProft, F., van Alsenoy, C., Peeters, A., Langenaeker, W. & Geerlings, P. (2002). *J. Comput. Chem.* **23**, 1198–1209.
Spackman, M. A., Byrom, P. G., Alfredsson, M. & Hermansson, K. (1999). *Acta Cryst.* A**55**, 30–47.
Stewart, R. F. (1976). *Acta Cryst.* A**32**, 565–574.
Stewart, R. F. & Bentley, J. (1975). *J. Phys. Chem.* **63**, 3786–3793.
Swaminathan, S., Craven, B. M. & McMullan, R. K. (1984). *Acta Cryst.* B**40**, 300–306.
Treutler, O. & Ahlrichs, R. (1995). *J. Chem. Phys.* **113**, 346–354.
Volkov, A., Li, X., Koritsánzky, T. & Coppens, P. (2004). *J. Phys. Chem. A*, **108**, 4283–4300.
Whitten, A. E. & Spackman, M. A. (2006). *Acta Cryst.* B**62**, 875–888.
Zarychta, B., Pichon-Pesme, V., Guillot, B., Lecomte, C. & Jelsch, C. (2007). *Acta Cryst.* A**63**, 108–125.